Supplementary Material for Turbulence in The Strongly Heterogeneous Near-Surface Boundary Layer over Patchy Snow

Michael Haugeneder* · Michael Lehning · Ivana Stiperski · Dylan Reynolds · Rebecca Mott

*WSL-Institute for snow and avalanche research SLF, michael.haugeneder@slf.ch

Spectra For All Sensors

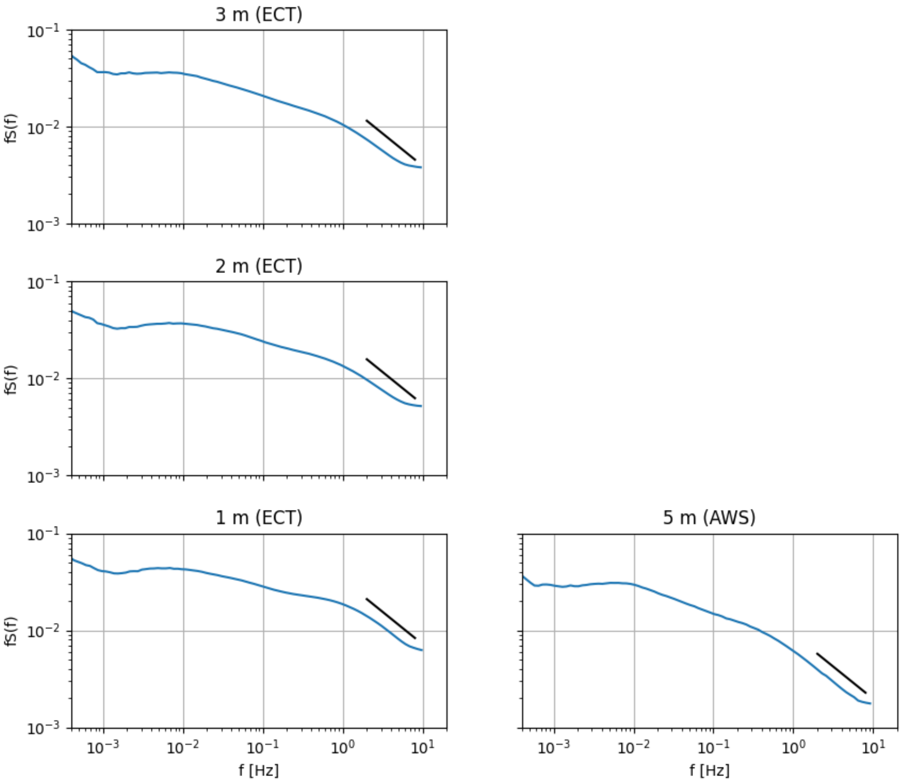

Fig. 16 Fourier-decomposed spectra of the sonic temperature T_s for all EC sensors over the whole observation period from 21 May to 11 June. The black lines indicate the theoretical $-\frac{2}{3}$ slope expected for the inertial subrange. An agreement indicates that the recorded data are trustworthy.

Föhn Diagnosis

To diagnose Föhn conditions during our observation period, we applied the mixture model from Plavcan et al. (2014). The model performs an unsupervised classification based on measured variables. In our case, we used the wind speed measured at the AWS as the primary classifier. Additionally, we took the potential temperature difference between the ridge station (see Fig. 1 for the location) and the AWS, the relative humidity measured at the AWS, and the wind direction at the AWS as concomitant classifiers. We used the foehnix-python package available on github (https://github.com/matthiasdusch/foehnix-python, accessed on 26 November 2023). Before applying the model, we filtered the AWS data and the data from the Grialetsch ridge station according to the prevailing wind directions. Only wind directions from the southern sector were selected as candidates for potential Föhn events.

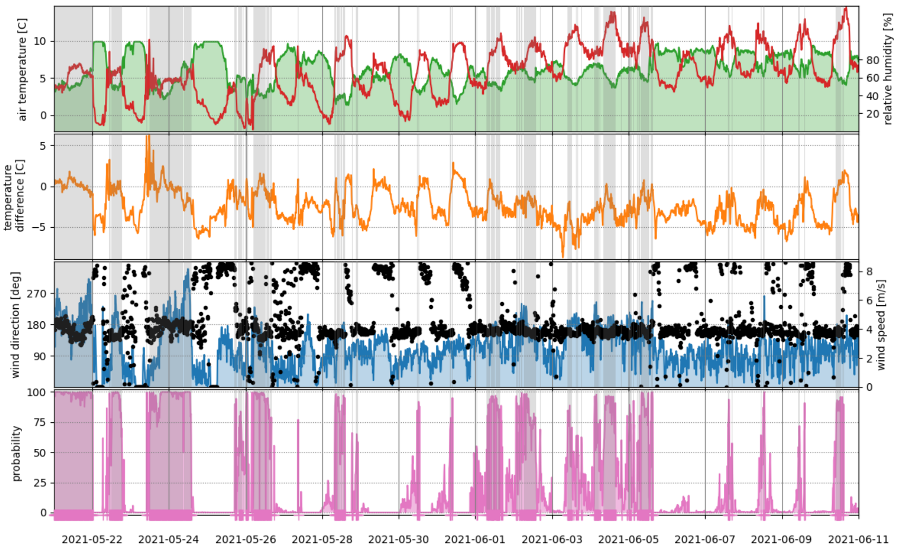

Fig. 17 Föhn diagnosis created with the foehnix-python package using the mixture model from Plavcan et al. (2014). The top panel shows the air temperature (red, left y-axis) and relative humidity (green, right y-axis) recorded at the AWS. The panel below depicts the potential temperature difference between the ridge station at Piz Grialetsch (see Fig. 1 for the location) and the AWS at Dürrboden. The next panel indicates the wind direction (black dots, left y-axis) and the wind speed (blue curve, right y-axis) at the AWS. The bottom panel displays the probability of Föhn according to the mixture model.

The probability panel shows that there was a Föhn event from the begin of the campaign (21 May to 24 May 1400 LT interrupted by two phases without Föhn. The model also classifies the period from 25 May 1800 LT to 26 May 1500 LT as Föhn. However, due to lack of power, the sensors at the ECT did not record data during this period and EC data cannot be analyzed. The following days are mostly recognized as non-Föhn days with short phases of increased probability of Föhn. Later, the period from 1 June 0000 LT to 5 June 1500 LT is dominated by Föhn with disruptions. Towards the end of the observation period, the model only classified short periods as Föhn. To sum up, for the analysis of the data in the present study the identified Föhn periods are

- 21 May 0000 LT to 25 May 1800 LT, interrupted twice
- 1 June 0000 LT to 5 June 1500 LT, high Föhn probability with disruptions

Multi-Resolution Flux Decomposition For All EC Sensors

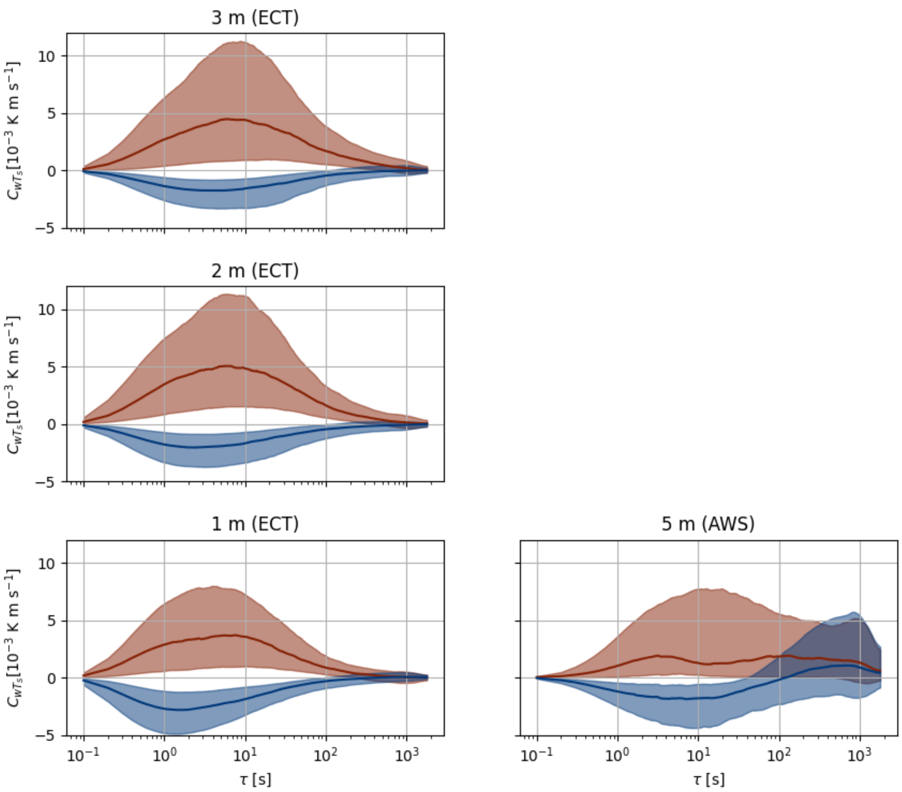

Fig. 18 Multi-Resolution Flux Decompositions for all EC sensors installed at Dürrboden during the observation period from 21 May to 11 June. The red curves correspond to unstable conditions, while the blue curves correspond to stable conditions.

Real Time Near-Surface Atmosphere Dynamics (Video)

An excerpt from a recorded thermal infrared sequence (31 May 2021 1445 LT) in real time is uploaded separately. Two thin, synthetic screens are deployed vertically across the transition from bare to snow. The screen's surface temperature serves as a proxy for the local air temperature (indicated by the colours) (Haugeneder et al. 2023). In the video, the up valley wind blows from left to right. The x-axis denotes the wind fetch distance over snow x, while the y-axis shows the height h above the bottom of the frame. The snow surface is shown in white.

The video visualizes the interaction between advected plumes of warm air and the stable internal boundary layer development over the snow surface in real time. The field of view is the same as in Fig. 9.